Analysis Predicted Location of Harmonic Distortion in RF Upconverter Structure

Sirmayanti Sirmayanti*[1], Mike Faulkner[2]
[1]Telecommunication Study Program, Electrical Department,
The State Polytechnic of Ujung Pandang, Indonesia
[2]College of Engineering and Science, Victoria University, Australia
*Corresponding author, e-mail: sirmayanti.sirmayanti@poliupg.ac.id

Abstract
A new mathematical analysis to predict the magnitude size of the distortion products from the signal up-conversion process output is presented. The signal up-conversion process converts the digital baseband from the analog baseband into a radio frequency signal. When the signal baseband involves frequency offsetting then occurring a number of distortion products which can reduce the dynamic range so it is difficult to meet the spectrum mask requirements within the operating band. This paper will focus on methods of new mathematical analysis using a continuous frequency range and only applies to a single side band tone, with constant amplitude into any value of frequency offsets. The novel contribution to the analysis starts at generating the gate signal and convolution of the gate signal into the reference carrier signal. The results show very close between the simulation results and the calculation of the predicted location of the distortions.

Keywords: baseband, upconverters, sigma-delta, harmonic, distortion

1. Introduction

Digital wireless transmission means an all-digital transmitter design. To move towards all-digital transmitter design so fully-digital components are required. Digital wireless transmission will support digital wireless system which its connectivity forces the development of wireless standards with higher energy efficiency incluiding wider bandwidth, higher data rate, linearity and signal dynamics. Traditional transceiver wireless device systems were mostly designed with radio frequency power amplfiers (RF-PAs) that still cannot be operated with a switching input waveform. Here, switched-mode power amplifier (SMPA) techniques in theoretically possible can improve power efficiency. However, SMPAs need to be driven by a pulse train generated from a polar representation of the transmitted baseband signal [1]. This has motivated to renewed interest in transmitter architectures based in a proposed Cartesian Sigma Delta (ΣΔ) transmitter architecture.

The most relevant work to the aims of this work was presented in [2]. In this model, the scheme operates a digital ΣΔ structure which replaces the analog components from the traditional transmitter architecture. The result at the baseband spectrum had shown the avoiding of bandwidth expansion by using a polar quantiser in a Cartesian structure. However, while reducing the bandwidth expansion, the Cartesian ΣΔ structure may still cause unwanted spectral components due to pulse width modulation/pulse position modulation (PWM/PPM) process. PWM/PPM techniques are used to control the amplitude and phase of an RF carrier. But, the rectangular nature of the output pulse generates a number of unwanted harmonics and distortion products such as an image, 3rd harmonic, -3rd harmonic and other low-odd order harmonics [3-5].

Bassoo *et al.* in [2] mathematically showed that a single side band (SSB) modulated tone causes distortion products and its results found that the PPM block was shown to be responsible for these distortions [2, 6]. For a single carrier environment, an increase in offset frequency also increases the unwanted spectral components. More other literatures, Routsalainen *et al.* in [7, 8] showed that larger frequency offsets caused image noise to fold in-band. They investigated a solution using complex noise shaping filters to move the main noise null and suppressing the image noise [7] and then another solution by using a fractional delay in the feedback path [8].

The management of distortion and noise is a key design challenge as is the requirement for tenability to achieve high efficiency transmission system. $\Sigma\Delta$ Techniques can shape the noise away from the carrier band for subsequent removal in a band-pass filter [9] and make it suitable for high-precision data acquisition applications [10], but tunability remains a problem [6]. Our previous work in [6], it describes a method of tuning which is particularly suitable for schemes with high-resolution polar quantisers, such as the waveform PWM-mode Cartesian $\Sigma\Delta$ [3-5]. The results recovers much of the dynamic range over the operating band.

This paper will focus on methods of mathematical analysis, which is carried out to determine the harmonic distortion at the output of the 'Polar to PWM/PPM' block, as shown in Figure 1. The approach in [2] will be followed with modifications to enhance the analysis. The novelty of the analysis will be discussed at section Results and Analysis (part 3.1 & 3.2).
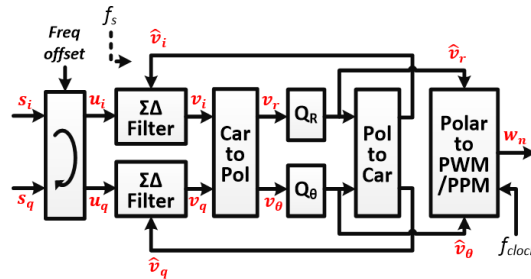

Figure 1. Cartesian $\Sigma\Delta$ scheme which is applied for baseband tuning scenario and odd quantisation scheme [3-6].

All distortion products reduce the dynamic range and it will making difficult to meet the spectrum mask requirements within the operating band. A number of distortion products (spurious signals) become apparent in the output spectrum from the 'polar to PWM/PPM' block. The mirrow image and harmonics occur caused by the rectangular pulse shapes fold in-band and cause interference to adjacent and nearby channels [6].

As we can see from Figure 1, the input signal of I-Q complex baseband, (s_i, s_q), is converted to polar representations, $R = \sqrt{I^2 + Q^2}$ and $\theta = \tan^{-1}\left(\frac{Q}{I}\right)$. $\Sigma\Delta$ filters independently are used to quantise the amplitude (R) and the phase (θ) signals respectively. The output of these quantisers $(\hat{v}_i, \hat{v}_q)$ is then fed back to their appropriate $\Sigma\Delta$ filter. Furthermore, the quantized signal $(\hat{v}_r, \hat{v}_\theta)$ is also sent through a 'Polar to PWM/PPM' block converter to generate the appropriate pulse waveform. Here, the final pulse train output of the 'Polar to PWM/PPM' (w_n) block will feed to the SMPA and band pass filter (BPF).

2. Research Method

The research method is based on the analysis results in [2] and technically we use the similar equation derivation (part 2.1) for the reference carrier signal $\tilde{S}_k(f)$ as shown in Figure 2 and Figure 3. Later, two scenarios for the odd quantisation [3-6] scheme and even quantisation [2] scheme are chosen for the comparison results.

The technique requires the carrier frequency (f_c) to be harmonically related to the number of clock frequency (f_{clock}). f_{clock} per nominal RF carrier period (f_c) sets the number of the availabily of quantisation points for the magnitude and phase quantisers, Q_R and Q_θ, respectively. The quantised amplitude ($\hat{v}_r$) is determined by the number of pulse widths or quantisation levels of N_A. The quantised phase ($\hat{v}_\theta$) is determined by the number of pulse positions or quantisation phases of N_P. The width and position of the pulse train are updated after K periods of the RF carrier. Factor K is a fixed relationship between the $\Sigma\Delta$ sample frequency, f_s, and the nominal carrier frequency f_c. We assume $K \geq 1$ (see (10) in [4]), so therefore

$$K = \frac{f_c}{f_s} \tag{1}$$

The mathematical analysis is based on a single SSB tone in which each an upper side band (USB) or lower side band (LSB) carrier is generated at frequency, $(f_c + f_{ssb})$ or $(f_c - f_{ssb})$ Hz respectively. The side band frequency, f_{ssb}, is determined by the phase slope $\left(\frac{\partial \theta}{\partial t}\right)$, so

$$f_{ssb} = \frac{1}{2\pi}\frac{\partial \theta}{\partial t} \qquad (2)$$

After quantisation with step size ($\Delta\theta$), the phase is actually linearly ramps up and changes to a staircase signal with oversampling ratio (OSR_{RF}) steps in *2π* radians, given by

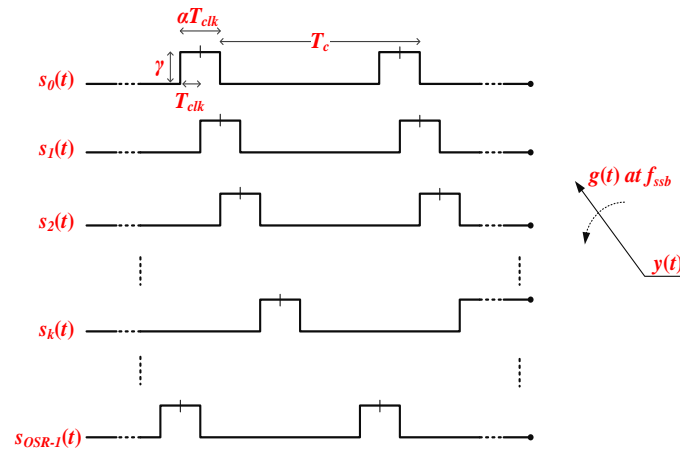$$\Delta\theta = \frac{2\pi}{OSR_{RF}} \qquad (3)$$

Figure 2. Phase shifted oscillators generate a SSB signal [2]

Figure 2 shows a SSB generation from a bank of phase-shifted oscillators. Each oscillator has an output of a quantised phase of $s(t)$. $s_0(t)$ is the first quantised phase then continuing by $s_k(t)$, where $k = 0, 1, \dots, (OSR_{RF} - 1)$. So, $s_1(t)$, for instance, is $s_0(t)$ delayed by T_{clk}. Each waveform, $s_k(t)$, is selected for a period by T_g. Therefore, there are OSR_{RF} clock periods in each carrier signal period, and it can be written as

$$T_c = T_{clk} \times OSR_{RF} \qquad (4)$$

Here, the expression for the output signal $s_k(t)$ is,

$$s_k(t) = s(t + kT_{clk}) \qquad (5)$$

During PWM/PPM process, the PWM maintains the pulse width constant (αT_{clk}) from the modulated amplitude and the PPM controls the increment (or decrement) of the pulse position from the modulated phase. As a result, all oscillators have the same pulse width, αT_{clk} at frequency f_c.

Moreover, there is a switch which rotates at a constant speed of f_{ssb} rotations/sec to obtain the output $y(t)$. The switch operates in a counter clockwise direction to delay the signal by 2π radians in T_{ssb} $\left(= \frac{1}{f_{ssb}}\right)$ seconds. The frequency of $y(t)$ is $(f_c - f_{ssb})$. The switch must rotate clockwise to give $f_c + f_{ssb}$ (USB). T_g is the duration that each of the OSR_{RF} oscillators is connected (or gated) to the output. So therefore,

$$T_g = \frac{T_{ssb}}{OSR_{RF}} \qquad (6)$$

Figure 2 is functionally similar to Figure 3 which shows the generation of SSB signal from the input $s(t)$ and $g(t)$, so the mathematical analysis can be expressed in more detail. The waveforms of $s_0(t)$ and $g_0(t)$ is respectively generated from the input reference oscillators by $s(t)$ and $g(t)$. Similarly to $s_k(t)$, the $g_k(t)$ gating waveform effectively selects each $s_k(t)$ output in turn, which is

$$g_k(t) = g(t + kT_g) \qquad (7)$$

So therefore, the output from the kth gate is given by

$$y_k(t) = s_k(t)\, g_k(t) \qquad (8)$$

and the total output $y(t)$ is the summation from all *OSR_RF* multiplexed output gates, giving by

$$y(t) = \sum_{k=0}^{\text{OSR}_{\text{RF}}-1} y_k(t) \qquad (9)$$

In this case, $\tilde{Y}(f) = F\{y(t)\}$ is calculated at the frequency domain using Fourier transform.
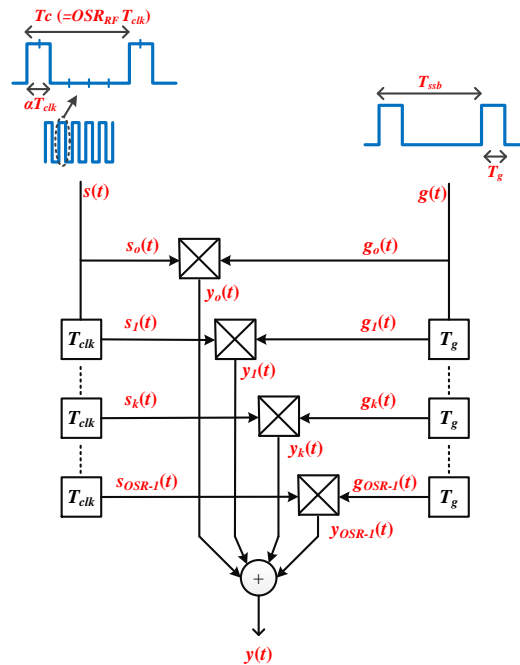

Figure 3. SSB generation for mathematical analysis [2]

2.1. The Reference Carrier Signal $\tilde{S}_k(f)$

$s_0(t)$ is the reference carrier signal. Since it is a repeating pulse signal so the properties of the discrete-time Fourier series method are used to calculate the spectrum. $s_0(t)$ can be formulated as

$$\tilde{S}_0(f) = \sum_{n=-\infty}^{\infty} S_0(n)\delta(f - nf_c) \qquad (10)$$

where

$$S_0(n) = \frac{\gamma \times \alpha T_{clk}}{T_c}\, sinc\left(\frac{n \times \alpha T_{clk}}{T_c}\right) \qquad (11)$$

is the Fourier series of pulse train of $s_0(t)$.

The *sinc* function on $S_0(n)$ aims to control the amplitude of the series of delta function at each the harmonics of f_c. Now $S_k(n)$ can be defined by using the time shifting property of the Fourier transform from $S_0(n)$

$$S_k(n) = S_0(n)e^{\frac{j2\pi nk}{OSR_{RF}}} \tag{12}$$

Therefore, the reference carrier signal with its the spectrum of the delayed waveform version can be written as

$$\tilde{S}_k(f) = \sum_{n=-\infty}^{\infty} S_0(n)e^{\frac{j2\pi nk}{OSR_{RF}}} \delta(f - nf_c) \tag{13}$$

3. Results and Analysis

3.1. The Gate Signal $\tilde{G}_k(f)$

The novel contribution to the analysis starts here. All the analysis at the previous results in [2] only apply to a few discere frequencies since it is assumed that the SSB gating waveform period is an integer number of samples. We now study all the analysis approach into any value of f_{ssb} (f_{offset}). As can be seen in Figure 4, it illustrates how to analyse the Gate Signal $\tilde{G}_k(f)$ condition.
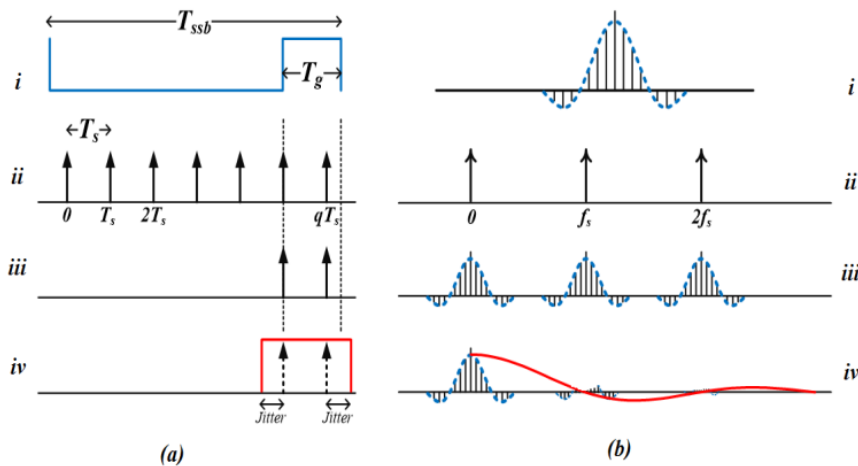

Figure 4. The gate signal generation. (a) in time domain, (b) in frequency domain, (i) input signal, (ii) sampling function, (iii) sample image, (iv) $\tilde{G}_0(f)$ output signal.

Note that $g_0(t)$ is defined as the edge of a SSB gating waveform. When it is not quantised on the sample grid, it experiences jitter. Figure 4 (i) illustrates the desired input gating, $g_0(t)$. The signal and the spectrum of $g_0(t)$ are discribed by the Fourier series of this repeating pulse $g_0(t)$ of period of T_{ssb}. $\tilde{G}_k(f)$ consists of harmonics of f_{ssb} ($=\frac{1}{T_{ssb}}$) weighted by a *sinc* function with nulls at $\frac{1}{T_g}$. $\tilde{G}_k(f)$ can be obtained by

$$\tilde{G}_k(f) = \sum_{n=-\infty}^{\infty} G_k(m)\delta(f - mf_{ssb}) \tag{14}$$

where

$$G_0(m) = \frac{1}{OSR_{RF}} sinc\left(\frac{m}{OSR_{RF}}\right) \tag{15}$$

and the delayed waveform version of $G_0(m)$ is written by

$$G_k(m) = G_0(m)e^{\frac{j2\pi mk}{OSR_{RF}}} \tag{16}$$

Futhermore, Figure 4(ii) shows the sampling function with period T_s which is the sample period of the ΣΔ. T_s is a series of impulses by $\sum_{q=0}^{\infty} \partial(t - qT_s)$. In other words, the spectrum of the sampling function is also a series of delta functions by $\sum_{p=0}^{\infty} \partial(f - pf_s)$. Figure 4 (iii) is obtained after the sampling process at the gating signal waveform of $g_0(t)$ resulting $\tilde{G}_k(f)$. Since both of them are in the time domain, so deriving the sampled spectrum of $\tilde{G}_k(f)$ is in multipication calculation, that is

$$\tilde{G}_k(f) = \sum_{p=-\infty}^{+\infty} \sum_{m=-\infty}^{+\infty} G_k(m)\, \partial(f - mf_{ssb} - pf_s) \tag{17}$$

Figure 4(iv) shows the jittered gating window. They are the time domain samples which are convolved with a square pulse of width T_s. Figure 4 (b) (iv) shows in detail their repeating spectrum in the frequency domain. Therefore, the total spectrum of the sampled gating signal, $\tilde{G}_k(f)$, is now multiplied by $T_s\, sinc\left(\pi\frac{f}{f_s}\right)$. $\tilde{G}_k(f)$ is formulated as

$$\tilde{G}_k(f) = T_s\, sinc\left(\pi\frac{f}{f_s}\right) \sum_{p=-\infty}^{+\infty} \sum_{m=-\infty}^{+\infty} G_0(m)e^{\frac{j2\pi mk}{OSR_{RF}}}\, \partial(f - mf_{ssb} - pf_s) \tag{18}$$

3.2. The Convolution of $\tilde{S}_k(f)$ and $\tilde{G}_k(f)$

In (8), the output $y_k(t)$ is obtained from the multipication (in time domain) of the reference carrier signal, $s_k(t)$, with the gating signal, $g_k(t)$. In frequency domain, $\tilde{Y}_k(f)$ is the convolution result of $\tilde{S}_k(f)$ and $\tilde{G}_k(f)$, that is

$$\tilde{Y}_k(f) = \tilde{S}_k(f) \otimes \tilde{G}_k(f) \tag{19}$$

Note that at the spectrum of $\tilde{G}_k(f)$, all its sampling images imprinted on each harmonic, nf_c, of the carrier pulse spectrum $\tilde{S}_k(f)$. As a result, the total of the spectrum is $\tilde{Y}(f)$ which is the sum of each gated phase spectrum of $\tilde{Y}_k(f)$.

Figure 5 illustrates the form of the spectra $\tilde{Y}(f)$. Figure 5 (a) is the series of carrier pulses with digital clock period T_c and with the Fourier transform that gives the harmonics at nf_c weighted by the *sinc* function of $S_0(n)\delta(f - nf_c)$ from (10). An example for the condition $OSR_{RF}= 8$ and $\alpha = 2$ (the pulse width is αT_{clk}) is decribed in Figure 5 (b). The zero crossing of the *sinc* function, z_c, is at

$$z_c = \frac{1}{\alpha \times T_{clk}} \tag{20}$$

or $\pm 4f_c$ for this example. Substituting (13) and (18) into (19), so therefore,

$$\tilde{Y}_k(f) = \sum_{n=-\infty}^{\infty} \begin{array}{c} S_0(n)e^{\frac{j2\pi nk}{OSR_{RF}}} \delta(f - nf_c) \\[4pt] \otimes \\[4pt] T_s\, sinc\left(\pi\frac{f}{f_s}\right) \sum_{p=-\infty}^{+\infty} \sum_{m=-\infty}^{+\infty} G_0(m)e^{\frac{j2\pi mk}{OSR_{RF}}}\, \partial(f - mf_{ssb} - pf_s) \end{array} \tag{21}$$

where *n*, *m*, and *p* are the harmonic bin number in the spectrum at f_c, f_{ssb} and f_s respectively. The total $\tilde{Y}(f)$ spectrum is the sum of each $\tilde{Y}_k(f)$, given by

$$\tilde{Y}(f) = \sum_{k=0}^{OSR_{RF}-1} \tilde{Y}_k(f) \tag{22}$$

Since $f_c = K f_s$ (see (10) in [4]) now we can see the images sit on top of each other (assumed K is 1). It is very clearly shown in Figure 5 (c) in the dotted green line that the signal

of interest is sitting at f_c, as well as the images of interest itself. A harmonic is occured only when $n + m = i \times OSR_{RF}$. n and m are the sample number harmonics at fc and fssb respectively and i is an integer. The exponential term sums to zero for all other combinations of n and m. Only when $m = (i \times OSR_{RF}) - n$, i.e $e^0 = 1$ so the output $\tilde{Y}(f)$ becomes:

$$\tilde{Y}(f) = \frac{OSR_{RF}}{f_s} \sum_{p=-\infty}^{+\infty} \sum_{n=-\infty}^{+\infty} \sum_{m=-\infty}^{+\infty} S_o(n)G_o(n) \, sinc\left(\pi \frac{(f-nf_c)}{f_s}\right)$$
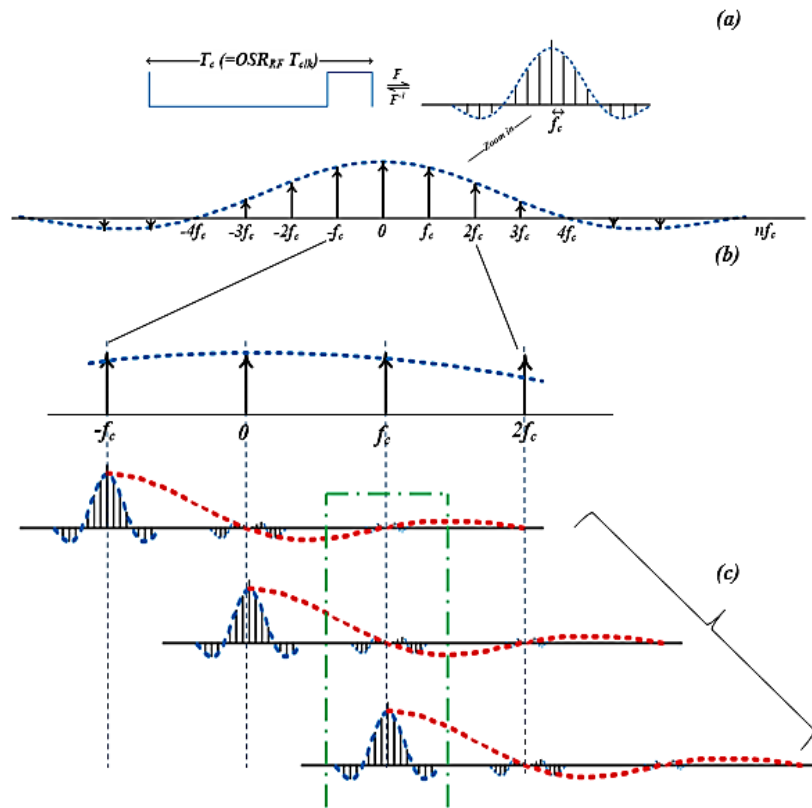$$\partial(f - nf_c - mf_{ssb} - pf_s) \tag{23}$$

Figure 5. The convolution of $\tilde{S}_k(f)$ and $\tilde{G}_k(f)$ gives $\tilde{Y}_k(f)$. (a) $\tilde{S}_k(f)$, (b) zoom of $\tilde{S}_k(f)$ with $OSR_{RF} = 8$ and $\alpha = 2$, (c) Summation of $\tilde{G}_k(f - nfc)$ that form $\tilde{Y}(f)$.

To predict the basic amplitude of the harmonic is given by $\frac{OSR_{RF}}{f_s} S_o(n)G_o(n)$. The condition of the delta function informs its position in the spectrum. The $sinc\left(\pi \frac{(f-nf_c)}{f_s}\right)$ weighting indicates that the interest in the spectrum is around f_c. Therefore, $nf_c + pf_s = f_c$ gives $K(n - 1) = -p$. This will be substituted into (23) that becomes:

$$\tilde{Y}(f_c + mf_{ssb}) = \tag{24}$$
$$\frac{OSR_{RF}}{f_s} \sum_{p=-\infty}^{+\infty} \sum_{n=-\infty}^{+\infty} \sum_{m=-\infty}^{+\infty} S_o(n)G_o(n) \, sinc\left(\pi\left(m\frac{f_{ssb}}{f_c} + (1 - n)\right)K\right)\partial(f - f_c - mf_{ssb})$$

An example result of value *n* and *m* is described. The first harmonic zone (f_c) is the location of the desired main SSB signal with $n = 1, m = -1, p = 0$; the image zone ($-f_c$) is with $n = -1, m = 1, p = -2K$; tThe 3rd harmonic zone ($f_c - 3f_{ssb}$) is with $n = 3, m = -3, p = 2K$; and the -3rd harmonic zone ($f_c + 3f_{ssb}$) is with $n = -3, m = 3, p = -4K$. An example of calculation results of the harmonics size with using each value above can be seen in Table 1.

Table 1. An Example of Calculation Results of the Harmonics Size

Harmonic size (dB)	Odd quantisation $\alpha = 5$, $\hat{v}_r = 0.6002$		Even quantisation $\alpha = 6$, $\hat{v}_r = 0.7074$	
	Simulation	Calculation	Simulation	Calculation
Image	29.6533	30.3703	29.821	30.3703
3rd harmonic	24.4384	24.9554	26.2643	26.5090

Table 1 shows the comparison between the simulation results of spectrum w_n and the calculation of the prediction location of the most dominant distortions: the image and the 3rd harmonic. The negative harmonic zone $(-f_c)$ is the image $(n = -1, m = 1, p = -2K)$ and the 3rd harmonic zone $(f_c - 3f_{ssb})$ is the 3rd harmonic $(n = 3, m = -3, p = 2K)$. Both the results are close. Agreement between simulation and calculation degrades as OSR_{RF} is reduced. Two scenarios for the odd quantisation [3-6] and even quantisation [2] are chosen for this comparison at values of $K = 1$, $f_{ssb} = 64$ MHz, $OSR_{RF} = 32$, and $f_c = 1024$ MHz. The pulse width, α, is based on the expected pulse width for a given input signal amplitude.

4. Conclusion

The extension of the mathematical derivation in [2] achieved results over a continuous frequency range rather than at a few spot frequencies. The new mathematical approach in this paper enabled the derivation of the prediction size of the magnitude of the distortion products. The analysis only applies to a SSB tone with constant amplitude. For modulated signals with varying phase and amplitude for instance, the high odd-order distortion products (3rd harmonic and above) become complex convolutions with smeared spectrum. So therefore, a different type of analysis is required for such signals. However, this expression still can be used to explain how the distortion products arise and considers techniques to cancel the image product and some of the noise enhancement cause by the intermediate frequency (IF) shift in [6].

References
[1] Sjöland H, Bryant C, Bassoo V, and Faulkner M. Switched-mode Transmitter Architectures. *Analog Circuit Design, Springer.* 2010: 325-342.
[2] Bassoo V, Linton L, and Faulkner M. Analysis of Distortion in Pulse Modulation Converters for Switching Radio Frequency Power Amplifiers. *IET Microwaves, Antennas & Propagation.* 2010; 4(12): 2088-2096.
[3] Sirmayanti S, Bassoo V, King H, and Faulkner M. *Odd-even quantisation and Cartesian delta-sigma (ΔΣ) Upconverters for Transmitter Design.* IEEE International Conference on Communication Systems (ICCS)*. Singapore. 2012: 100-104.*
[4] Sirmayanti S, Bassoo V, King H, and Faulkner M. *OFDM Performance with Odd-Even Quantisation in Cartesian ΔΣ Upconverters.* IEEE International Conference on Signal Processing and Communication Systems. Gold Coast Australia. 2012: 1-5.
[5] Sirmayanti S, Bassoo V, Faulkner M. *Joint Odd-Even Quantisation in Cartesian Delta-Sigma (ΔΣ) Upconverters.* IEEE Africon*. Pointe-Aux-Piments Mauritius. 2013: 1-4.
[6] Sirmayanti S, Bassoo V, King H, and Faulkner M. Baseband Tuning of Cartesian Delta–Sigma RF upconverters. *IET Electronics Letters Journal.* 2014; 50(8): 635–637.
[7] Ruotsalainen H, Arthaber H, Magerl G. A New Quadrature PWM Modulator With Tunable Center Frequency for Digital RF Transmitters. *IEEE Transactions on Circuits and Systems II: Express Briefs.* 2012; 59(11): 756-760.
[8] Ruotsalainen H, Arthaber H, Magerl G. *Quantization noise cancelation scheme for digital quadrature RF pulse encoding.* IEEE MTT-S International Microwave Symposium Digest (MTT). Seattle, WA. 2013: 1-4.
[9] Schreier R, Temes G C, Wiley J. *Understanding Delta-sigma Data Converters.* 74. New Jersey: IEEE Press Piscataway. 2005.
[10] Shu-jing S U, Hai-li, Z H A N G. The Study and Achieving of High-precision Data-acquisition Based on ΔΣADC. *Indonesian Journal of Electrical Engineering and Computer Science.* 2013; 11(8): 4453-4460.